THE JOURNAL OF PHYSICAL CHEMISTRY C

Article

pubs.acs.org/JPCC

Understanding Deviations in Hydrogen Solubility Predictions in Transition Metals through First-Principles Calculations

Kyoungjin Lee, Mengyao Yuan, and Jennifer Wilcox*

Department of Energy Resources Engineering, Stanford University, 367 Panama Street, Stanford, California 94305, United States

Supporting Information

ABSTRACT: Hydrogen solubility in ten transition metals (V, Nb, Ta, W, Ni, Pd, Pt, Cu, Ag, and Au) has been predicted by first-principles based on density functional theory (DFT) combined with chemical potential equilibrium between hydrogen in the gas and solid-solution phases. Binding energies and vibrational frequencies of dissolved hydrogen in metals are obtained from DFT calculations, and the sensitivity of solubility predictions with respect to the DFT-calculated variables has been analyzed. In general, the solubility increases with increasing binding strength and decreasing vibrational frequencies of hydrogen. The solubility predictions match experimental data within a factor of 2 in the cases of V, Nb, Ta, and W and within a factor of 3 in the cases of Ni, Cu, and Ag. In Pd, the deviation in solubility predictions is mainly attributed to the errors involved in the calculated vibrational frequencies of dissolved hydrogen. In Pt and Au, hydrogen in the octahedral interstitial site is less stable than in the tetrahedral site, contradicting the predictions based on the hard-sphere model. Potential energy surface analysis reveals a slightly downward concavity near the center of the octahedral sites in Pt and Au, which may explain the calculated imaginary vibrational frequencies in these sites and lead to unreliable solubility predictions.

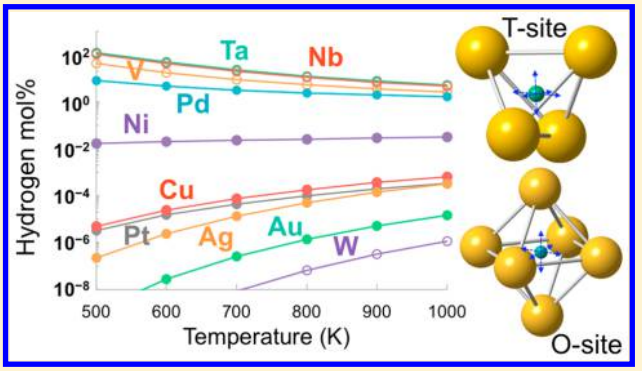

1. INTRODUCTION

Hydrogen is a promising clean energy carrier compared to fossil fuels since neither pollutants nor carbon dioxide (CO_2) is emitted upon its combustion. However, the production and purification of hydrogen are energy-intensive processes and currently rely on fossil fuels. To improve efficiencies of hydrogen production and purification and to mitigate associated greenhouse gas emissions, understanding hydrogen absorption and diffusion in metals would be valuable for many practical problems such as hydrogen separation using metallic membranes[1−5] and preventing hydrogen-induced embrittlement (HIE) in industrial facilities. In metallic membranes, hydrogen permeability, defined as the product of the solubility and diffusivity, is directly related to the separation capability of membranes. While both high solubility and high diffusivity are desired, one may screen membrane materials based on solubility first, particularly in the cases of BCC metals, where the solubility is thought to play a more dominant role in determining the permeability.[2,6] Besides, high hydrogen solubility may induce HIE, which is a critical issue for the structural stability of membranes. HIE refers to the mechanical failure of metals due to lattice expansion, distortion, and fracture caused by absorbed hydrogen.[7,8] While embrittlement mechanisms vary with the microstructure of materials, those with high hydrogen solubility have a general tendency to easily become brittle. For desirable membrane performance, the hydrogen solubility should be tuned properly to achieve a maximum solubility while suppressing HIE.[2]

While hydrogen solubility in transition metals at various temperatures has long been investigated by various experimental methods,[9−15] material and equipment costs as well as the long time span of equilibration can sometimes be a limiting factor for the experimental studies. Theoretical modeling may help avoid cost and time constraints by predicting the hydrogen solubility and thereby allowing for a greater understanding of hydrogen binding in metals from atomic-scale perspectives. Thermodynamic modeling was first established alongside experimental measurements.[12,16−19] Hydrogen solubility is treated as an equilibrium constant associated with the chemical equilibrium between gaseous hydrogen and dissolved hydrogen in a solid solution. With the assumption of a quasi-regular interstitial solution, a linear relationship between the log of the solubility and the inverse temperature has been observed.[20] From the extrapolated linear relationship, the enthalpy and entropy of hydrogen dissolution can be obtained from the slope and the intercept on the log axis, respectively. These thermodynamic variables have been further modeled as a function of hydrogen solubility[12,17] or the lattice constant of the alloys.[18]

Received: June 8, 2015
Revised: July 27, 2015
Published: August 10, 2015

DOI: 10.1021/acs.jpcc.5b05469
J. Phys. Chem. C 2015, 119, 19642−19653

Electronic structure studies on hydrogen-absorbed metal systems have provided a more profound understanding of hydrogen absorption in metals and alloys.[6,19−24] It has been understood that hydrogen can bind in metal interstitial sites or defects (e.g., vacancies and grain boundaries), where the added electron from hydrogen fills the metal d-band of neighboring atoms and the electron density associated with hydrogen becomes closer to an optimal level.[20,24] In recent studies, first-principles based on density functional theory (DFT) have been directly applied to the calculation of macroscopic thermodynamic properties such as heat and entropy of dissolution and accordingly the solubility of hydrogen in metals. The simplest structure of hydrogen in transition metals is the case of interstitial hydrogen. On the basis of the interstitial model, the solubility of hydrogen in various transition metals has been predicted, including in Pd,[25,26] Pd-based alloys (e.g., PdCu,[26−30] PdAg,[28,29] PdAu,[28] and PdRh[29]), W,[31,32] Mo,[25,33] Cu,[25,34] and other metals.[25] The predictions have shown a similar trend to experimental results, but some discrepancies remain to be fully explained. In theory, the predicted results may be affected by the simplicity of the interstitial model structure in describing realistic systems or by intrinsic errors associated with DFT calculations. Many studies indeed have reported that hydrogen binding in a metal vacancy or within grain boundaries is generally much stronger than one in an interstitial site.[25,31,35−39] However, vacancy formation energy is often omitted when hydrogen binding strength is compared within various hydrogen−vacancy complexes, which has led to a biased idea that vacancy binding might be predominant in hydrogen dissolution in metals. Formation of a vacancy from a perfect crystal requires energy input, resulting in the number of vacancies being much smaller than the number of available interstitial sites.[25] While enhanced vacancy formation has been reported in the presence of hydrogen, and consequently superabundant vacancy formation has been reported in certain circumstances,[37−41] a major contribution to the total hydrogen solubility seems to be the interstitial trapping of hydrogen.[25] In this regard, using a simple interstitial model for dilute solutions can be a valid approach. The deviations of solubility predictions from experiments then may be attributed to the accuracy of DFT-calculated variables to some extent. DFT results are provided in the literature often without an error range, although convergence is achieved in individual studies. Since these DFT results are used in subsequent thermodynamic equilibrium calculations to obtain solubility values, understanding the variations in DFT values would provide useful information to solubility predictions.

In this study, we have calculated hydrogen solubility in metals based on chemical potential equilibrium with a quasi-regular interstitial solution, where DFT-calculated binding energy and vibrational frequency of hydrogen in metals are crucial variables in determining the chemical potential of dissolved hydrogen. In particular, we will show the sensitivity of solubility predictions to those of two DFT-calculated variables. Subsequently, the accuracy of the DFT calculations will be discussed, followed by solubility predictions and comparisons to experimental values for the following 10 early and late transition metals: vanadium (V), niobium (Nb), tantalum (Ta), tungsten (W), nickel (Ni), Pd, platinum (Pt), copper (Cu), silver (Ag), and gold (Au). Finally, case studies on the metals for which the solubility predictions significantly deviated from the experimental values will be further discussed.

2. METHODS

Derivation of the solubility from thermodynamic equilibrium is described in the Supporting Information. In short, binding energy and vibrational frequencies of atomic hydrogen in an interstitial site obtained from first-principles calculations will be used to calculate hydrogen solubility in a metal. First-principles calculations based on DFT[42,43] were performed using the Vienna *ab initio* Simulation Package (VASP, v5.2.12)[44−47] with the projector-augmented wave (PAW) method[48,49] to describe nucleus−electron interactions. Electron exchange-correlation functionals were represented with the generalized gradient approximation (GGA) using the model of Perdew, Burke, and Ernzerhof (PBE).[50,51] Plane waves with the kinetic energy cutoff of 450 eV were used to describe electronic wave functions, and the Monkhorst−Pack scheme[52] was applied for the sampling of k-points in a k-space of 8 × 8 × 8. While the electronic energy in the self-consistent field was converged below 10^{-7} eV, the total energy convergence to within 1 meV/atom was achieved with respect to the energy cutoff and k-point parameters. The first-order Methfessel and Paxton smearing method[53] with a width of 0.2 eV was used for the Fermi-level integration. We performed geometry optimization with a fully relaxed cell volume for each metal. For V, Nb, Ta, and W, a 2 × 2 × 2 conventional BCC supercell (16 atoms) was used, and for Ni, Pd, Pt, Cu, Ag, and Au, a 2 × 2 × 2 conventional FCC supercell (32 atoms) was employed. Spin-polarized calculations were applied to Ni and Pd. After the geometry optimization of pure metal lattices, we fixed the lattice and added one hydrogen atom in an interstitial binding site per supercell. The hydrogen-to-metal ratio chosen in this study is suitable to describe a dilute solution with a reasonable amount of computational resources (e.g., hydrogen binding energies in the O-site of 108 atoms of Cu, Pt, and Au differ by 0.01−0.02 eV/H compared to those of 32 atoms). All ionic positions were relaxed using the conjugate-gradient algorithm so that the absolute values of the forces on unconstrained atoms became less than 0.01 eV/Å. From the optimized structure, we calculated the normal-mode vibrational frequencies of the hydrogen atom by a finite displacement method with a displacement size of 0.015 Å. We calculated the energy of the H_2 molecule in the gas phase by placing one H_2 in a 20 × 20 × 20 $Å^3$ cubic box and choosing the Γ-point. The binding energy (BE) of atomic hydrogen in an interstitial binding site with respect to gaseous H_2 was calculated by taking the total energy difference between the initial (pure metal and the hydrogen molecule in the gas phase) and final state (one hydrogen bound in an interstitial site of the metal)

$$\mathrm{BE} = E(\mathrm{M} + \mathrm{H}) - E(\mathrm{M}) - \frac{1}{2}E(\mathrm{H_2}) \tag{1}$$

such that $E(\mathrm{M} + \mathrm{H})$, $E(\mathrm{M})$, and $E(\mathrm{H_2})$ are the total energies of hydrogen-absorbed metal, the bulk metal, and hydrogen in the gas phase, respectively.

Zero-point energies (ZPEs) should be taken into account in a system of light atoms such as hydrogen, where the quantum wavelength (de Broglie wavelength) exceeds the atomic separation. The ZPE-included binding energy is defined as eq 2

$$\mathrm{BE_{ZPE}} = \mathrm{BE} + \Delta\mathrm{ZPE} = \mathrm{BE} + \left\{\mathrm{ZPE(M + H)} - \mathrm{ZPE(M)} - \frac{1}{2}\mathrm{ZPE(H_2)}\right\} \tag{2}$$

DOI: 10.1021/acs.jpcc.5b05469
J. Phys. Chem. C 2015, 119, 19642−19653

where ZPE is given by eq 3

$$\mathrm{ZPE} = \sum_i \frac{h\nu_i}{2} \tag{3}$$

for each vibrational frequency ν_i associated with the vibrational mode i for all real vibrational modes present. Since our results showed that the vibrations of the bulk metal (phonons) are negligible compared to the atomic hydrogen vibration in an interstitial site, the ZPM (M) was ignored, and ZPM (M + H) was replaced with ZPE (H). Since the atomic hydrogen is confined in an interstitial site, the three degrees of freedom in the motion of the hydrogen would correspond to three normal modes of vibration.

3. RESULTS AND DISCUSSION

3.1. Sensitivity of Solubility Prediction Parameters. In our solubility prediction model, the binding energy and vibrational frequency of interstitial hydrogen are the only unknown variables calculated by DFT. Before discussing the DFT results in the next section, we performed a sensitivity analysis showing how solubility would change with respect to hypothetical values of the binding energy and vibrational frequency. Figure 1 shows the hydrogen solubility as a function

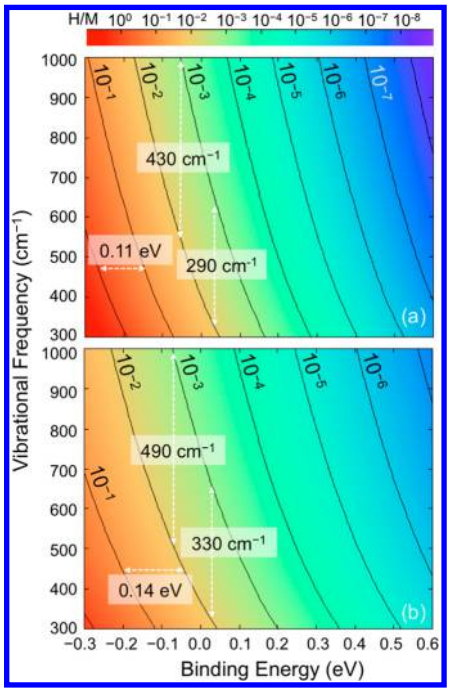

Figure 1. Hydrogen solubility as a function of binding energy and vibrational frequency in the O-site of the FCC metals at (a) 600 K and (b) 800 K. The magnitude of solubility (ratio of hydrogen atoms to metal atoms) is indicated by the color bar and the contour lines on the plots.

of binding energies (as defined in eq 1, without ZPEs) and vibrational frequencies associated with the O-site of an FCC metal, in which the ratio of the number of binding sites to that of metal atoms is unity, and the three vibrational frequencies are identical.

One can notice that the solubility generally increases as the binding becomes stronger or the vibrational frequency decreases. It intuitively makes sense that a stronger binding leads to a higher solubility, as more hydrogen will be absorbed in the metal due to the strong affinity. Vibrational frequencies of atomic hydrogen in metals contribute to the solubility through the vibrational partition function that ultimately determines the energy of hydrogen absorption. According to eq S8 (shown in the Supporting Information), smaller vibrational frequencies result in a larger vibrational partition function, leading to a higher solubility. In the following sections, one will notice that smaller vibrational frequencies are generally observed where a hydrogen atom is bound in a more spacious interstitial site, e.g., the O-site of the FCC metals compared to the T-site of the BCC metals. However, despite the larger contribution from the vibrational frequencies in the FCC metals, the hydrogen solubility is generally greater in the BCC metals due to the strong binding of hydrogen.

Since the accuracy of the binding energy and vibrational frequency calculations is crucial to the solubility prediction, it would be useful to have a quantitative understanding of the error ranges in the binding energy and vibrational frequency that would result in an order of magnitude difference in the predicted solubility. Figure 1(a) indicates that an error of 0.11 eV in the binding energy at a fixed vibrational frequency or an error of 290−430 cm^{-1} in the vibrational frequency at a fixed binding energy corresponds to an order of magnitude error in the solubility. The solubility change is more sensitive to lower vibrational frequencies, implied by the steeper slope with respect to the vibrational frequency in the solubility contour plots. This higher sensitivity is due to the vibrational partition function decreasing more rapidly at lower vibrational frequencies (according to eq S8 in the Supporting Information). Thus, when the vibrational frequency of atomic hydrogen is relatively low, the errors in the solubility prediction are attributed to two factors: (i) the higher sensitivity of solubility to vibrational frequency at lower frequencies and (ii) larger relative errors at lower frequencies due to absolute intrinsic errors in the DFT calculations. For these reasons, errors in the vibrational frequencies seem to play a significant role in the solubility predictions in the case of Pd (see Section 3.4). Figure 1(b) presents a similar sensitivity plot for 800 K. The contour levels are more widely spaced than those shown in Figure 1(a), indicating that the solubility is less sensitive to the variations in the binding energy and vibrational frequency at a higher temperature due to an increased contribution of the vibrational partition function. At 800 K, an error of 0.14 eV in the binding energy or 330−490 cm^{-1} in the vibrational frequency induces an order of magnitude error in the solubility.

Despite the errors in the DFT-predicted binding energy and vibrational frequency, in cases where the effects cancel each other, the resulting error in the calculated solubility may become negligible. Nevertheless, it is important to calculate each variable in DFT with high accuracy for consistent solubility predictions. In the next section, we will discuss the DFT results in greater detail.

3.2. Binding Energy of Interstitial Hydrogen in Metals. The predicted lattice constants are compared against experiment in Table 1. The errors in the predictions are within ±2.3%, and all the lattice constants have been overestimated, with the exception of V. The overestimation of the lattice constants is a well-known trend for the GGA-PBE exchange-correlation functional.[54,55] In Table 2, we show the binding energies predicted by first-principles calculations using the optimized lattice constants of the metals. We defined the binding energy such that a negative binding energy indicates thermodynamically favorable absorption. Conversely, a positive

DOI: 10.1021/acs.jpcc.5b05469
J. Phys. Chem. C 2015, 119, 19642−19653

Table 1. Lattice Constant Predictions from First-Principles Calculations and Interstitial Radii Estimated by the Hard-Sphere Model[a]

metal	group	cubic structure	experimental lattice const.[67] (Å)	predicted lattice const. (Å)	atomic radii (Å)	T-site radii (Å)	O-site radii (Å)
V	5	BCC	3.02	2.995	1.31	**0.38**	0.20
Nb	5	BCC	3.30	3.32	1.43	**0.42**	0.22
Ta	5	BCC	3.30	3.32	1.43	**0.42**	0.22
W	6	BCC	3.16	3.19	1.37	**0.40**	0.21
Ni	10	FCC	3.52	3.52	1.24	0.28	**0.52**
Pd	10	FCC	3.89	3.96	1.38	0.31	**0.58**
Pt	10	FCC	3.92	3.98	1.39	0.32	**0.58**
Cu	11	FCC	3.61	3.63	1.28	0.29	**0.53**
Ag	11	FCC	4.09	4.16	1.45	0.33	**0.61**
Au	11	FCC	4.08	4.17	1.44	0.33	**0.61**

[a]The values in bold indicate the size of the interstitial site where hydrogen binding is preferred based on the hard-sphere model.

Table 2. Binding Energy and Vibrational Frequency of Atomic Hydrogen in Metals Predicted by First-Principles Calculations

	binding energies (eV/H)		vibrational frequencies (cm^{-1})	
metal	T-site[b]	O-site[b]	T-site	O-site[a]
V	−0.30	−0.06	1529.4, 1529.3, 1016.3	2423.3, 701.8*i*, 702.2*i*
	(−0.19)	(−0.05)		
Nb	−0.34	0.03	1392.0, 1391.3, 1008.6	2335.2, 799.1*i*, 799.6*i*
	(−0.24)	(0.03)		
Ta	−0.35	0.04	1414.5, 1414.4, 1034.6	2384.7, 841.0*i*, 841.3*i*
	(−0.25)	(0.05)		
W	0.94	1.37	1530.6, 1530.3, 1156.0	2569.9, 915.4*i*, 915.4*i*
	(1.06)	(1.39)		
Ni	0.35	0.08	1288.4, 1287.8, 1287.7	804.5, 804.3, 803.9
	(0.45)	(0.09)		
Pd	−0.04	−0.09	990.7, 990.4, 990.0	315.0, 314.4, 313.8
	(0.00)	(−0.17)		
Pt	0.53	0.58	944.8, 944.5, 944.5	397.3*i*, 397.3*i*, 397.3*i*
	(0.57)	(0.45)		
Cu	0.64	0.45	1169.1, 1168.8, 1168.7	713.5, 713.5, 713.3
	(0.72)	(0.44)		
Ag	0.72	0.68	867.6, 867.5, 867.5	380.7, 380.2, 380.2
	(0.75)	(0.61)		
Au	0.84	1.03	695.6, 695.4, 695.3	448.9*i*, 449.8*i*, 449.7*i*
	(0.83)	(0.89)		

[a]*i*: Imaginary number. [b]Values shown in parentheses are ZPE-corrected binding energies.

binding energy indicates that hydrogen absorption is thermodynamically unfavorable. By this definition, the lower the binding energy, the stronger the interaction. DFT-predicted binding energies (with and without ZPE correction) are also listed in Table 2.

The binding energies we predicted are in reasonable agreement with previous theoretical predictions from the literature. Compared to hydrogen binding energies in the T- and O-sites of bulk V, Nb, and Ta calculated from first-principles in Aboud and Wilcox,[56] Ouyang and Lee,[57] and Sundell and Wahnstrom,[58] our results differ by a maximum of 0.12 eV/H. Our hydrogen binding energy in the T-site of W agrees with the values reported in the literature to within 0.08 eV/H.[31,32,35,59−62] Hydrogen in the O-site of these BCC metals is known to exist at a high-order saddle point,[57,62,63] which is consistent with our findings (see further details in Section 3.3). In the case of Ni, the binding energies predicted in this study are lower by 0.09−0.14 eV/H than those found in the literature.[25,39,64] In the cases of Pd[25,26,39,65] and Ag,[39] our calculated binding energies are different within 0.06 eV/H compared to the literature. Hydrogen binding energies in Cu,[25,34,39] Pt,[39] and Au[39] reported in the literature vary from our results within 0.09, 0.09, and 0.12 eV/H, respectively. Much larger differences in the range of 0.3−0.4 eV are found between our hydrogen binding energy results for the O-sites of Pd, Pt, and Au and those in Yokoi et al.,[66] yet since neither exact numerical data nor computational details are available in this previous study, it is difficult to make a fair comparison. On the basis of the sensitivity analysis presented in Section 3.1, the binding energies calculated in this study are expected to give reasonable predictions of solubility, i.e., within 1 order of magnitude difference.

A general trend observed from experimental evidence is that hydrogen tends to occupy the T-sites in the BCC lattice and O-sites in the FCC lattice.[9,17,20] Here, we make an attempt to explain the mechanism of the observed site preference from the hard-sphere model and our DFT predictions and discuss two exceptions to this trend. On the basis of the hard-sphere model and the predicted lattice constants, the radii of the T- and O-sites were estimated, as shown in Table 1. Given the covalent radius of the hydrogen atom, 0.25 Å,[68] the size of the T-sites (0.38−0.42 Å) in the BCC metals is sufficient to contain a

DOI: 10.1021/acs.jpcc.5b05469
J. Phys. Chem. C 2015, 119, 19642−19653

hydrogen atom, but the O-sites (0.20−0.22 Å) in the BCC metals would be too small. In the case of the FCC metals, the T-sites (0.28−0.33 Å) can tightly fit a hydrogen atom, whereas the O-sites (0.52−0.61 Å) are sufficiently large. On the basis of this size argument, hydrogen binding in the BCC metals would be more favored in the T-site than in the O-site. Either the T- or O-site may be occupied by hydrogen in the FCC metals, but hydrogen binding may be particularly favored within an optimally sized interstitial site, which can be provided by the O-site. The more spacious O-site in the FCC metals would be able to offer stronger binding, in general, than the constricted T-site. Small interstitial sites tend to result in weak binding since interstitial binding causes a high energy penalty associated with lattice expansion or distortion.

However, the size is not the only factor determining the site preference. We found little quantitative correlation between the magnitude of the hydrogen binding energy and the size of the interstitial site predicted from the hard-sphere model. For example, W has a similar T-site radius to that of V, Nb, and Ta, but the binding energy in W is notably different from those in the Group 5 metals. In addition, the pairs of Ni and Cu, Pd and Pt, and Ag and Au have similar O-site radii (differing by 3.1%, 0.5%, and 0.3%, respectively), but the hydrogen binding energy in these metal pairs has a wide range (differing by 83%, 116%, and 34%, respectively). Only within the Group 5 metals, which have similar lattice constants, are the binding energies close to each other. This trend confirms that the site preference of hydrogen in metals cannot be predicted solely by the interstitial size based on the hard-sphere model. The hard-sphere model served as a basis for some previous studies[69,70] on hydrogen solubility in metals, where the hydrogen site preference cannot be accurately measured by experiments due to very low solubility of hydrogen. The electronic structure of the metal associated with the binding sites may play a significant role[21,23,24] even in a relatively simple pure metallic system such as the ones presented in this study.

Another exception to the site preference observed from experiments and deduced by the hard-sphere model is hydrogen binding in Pt and Au. Hydrogen binding in the O-site is expected for FCC metals, but our binding energy calculations from DFT indicate that the T-site is preferred in Pt and Au, both having an FCC structure. Previous DFT-based calculations[38,39] also showed that the T-site is preferred for hydrogen binding in Pt and Au; however, You et al.[38] did not provide an explanation for this unexpected phenomenon, and the results from Nazarov et al.[39] are different from ours to the extent that hydrogen is stable in the O-site of Pt when the zero-point vibration is considered. We will discuss this unclear site preference in Au and Pt further in Section 3.5.

3.3. Normal-Mode Frequency of Interstitial Hydrogen in Metals. The calculation results of the normal-mode vibrational frequencies are listed in Table 2. The values are truncated to the tenths place for convenience. One indication of the numerical accuracy with respect to the size of displacement in the finite displacement method is that very similar numbers for the three equivalent vibrational modes in the FCC O-sites were observed (standard deviation of 0.6 cm^{-1}), whereas a deviation of a few cm^{-1} among the equivalent vibrational modes would result otherwise. Still, this measure of accuracy does not necessarily include the errors associated with the geometry optimization in our DFT model. Therefore, some deviations from experimental results are expected, which is common in DFT calculation.[71]

As explained in the Methods section, normal-mode vibrational frequencies (Table 2) were used to calculate the vibrational partition function in the solubility equation. According to eq 2, if the ZPE of the interstitial hydrogen atom, ZPE (H), is smaller than half of the ZPE of hydrogen gas, 1/2ZPE (H_2), the effect of the net ZPE to the binding energy will be to strengthen the binding. In the BCC metals, the net ZPE weakens the binding in the T-site more significantly than in the O-site, so that the ZPE-corrected binding energy difference between the O- and T-sites becomes smaller. In the FCC metals, on the other hand, the O-site binding is generally strengthened by the net ZPE, whereas the T-site binding is weakened, so that the ZPE-corrected binding energy difference between the two sites becomes greater. From this point of view, ZPEs play an important role in determining the site preference of interstitial hydrogen.

Shown in Table 2, the three vibrational frequencies of atomic hydrogen in each of the four BCC metals investigated in this study share a similar trend. Two of the frequencies associated with the vibration in the T-site are higher than the third due to the lack of T-site symmetry along one axis compared to the regular tetrahedron. The hydrogen vibration in the BCC metals' O-site involves two imaginary frequencies, indicating that the O-site is not the true energy minimum on the potential energy surface (PES) but is a second-order saddle point. Similar saddle-point behaviors of hydrogen in the O-site of BCC metals have also been reported in the literature.[57,62,63,72] The presence of imaginary vibrational modes in the BCC O-sites indicates the unstable nature of the binding and supports the site preference deduced from the binding energy and interstitial size as discussed in Section 3.2.

In the FCC metals, the three normal-mode vibrational frequencies of hydrogen for each of the O-site or T-site binding are almost identical due to the octahedral or tetrahedral symmetry associated with the interstitial sites. Pt and Au showed three imaginary frequencies for the hydrogen vibration in the O-site, indicating that the optimized geometry of hydrogen binding in the O-site is not at the true energy minimum. These results are consistent with the binding energy results, which demonstrated that binding in the T-site is more favorable than that in the O-site. Since hydrogen binding in these two metals is distinguished from that in the other FCC metals, further investigation of Pt and Au has been carried out and is discussed in Section 3.5.

3.4. Prediction of Hydrogen Solubility in Metals. Using the binding energies and vibrational frequencies from the first-principles calculations, we predicted the hydrogen solubility in the 10 metals. Figure 2 shows our solubility predictions and corresponding experimental values reported in the literature. The solubility in this study is expressed as a ratio of the number of hydrogen atoms to the number of metal atoms (H/M). We show two solubility predictions for each metal: assuming the O-site binding dominates the solubility and assuming the T-site binding dominates.

In most cases, we observed that the experimental solubility in each metal is closer to the higher solubility value predicted for the two sites, indicating that one of the two binding sites dominates the bulk solubility. The site that appears to dominate the solubility corresponds to the one in which a stronger binding is demonstrated. In other words, the hydrogen solubility in the BCC metals is dominated by T-site binding, whereas in the FCC metals with the exception of Pt and Au the O-site binding dominates. In Pt, since the solubility associated

DOI: 10.1021/acs.jpcc.5b05469
J. Phys. Chem. C 2015, 119, 19642−19653

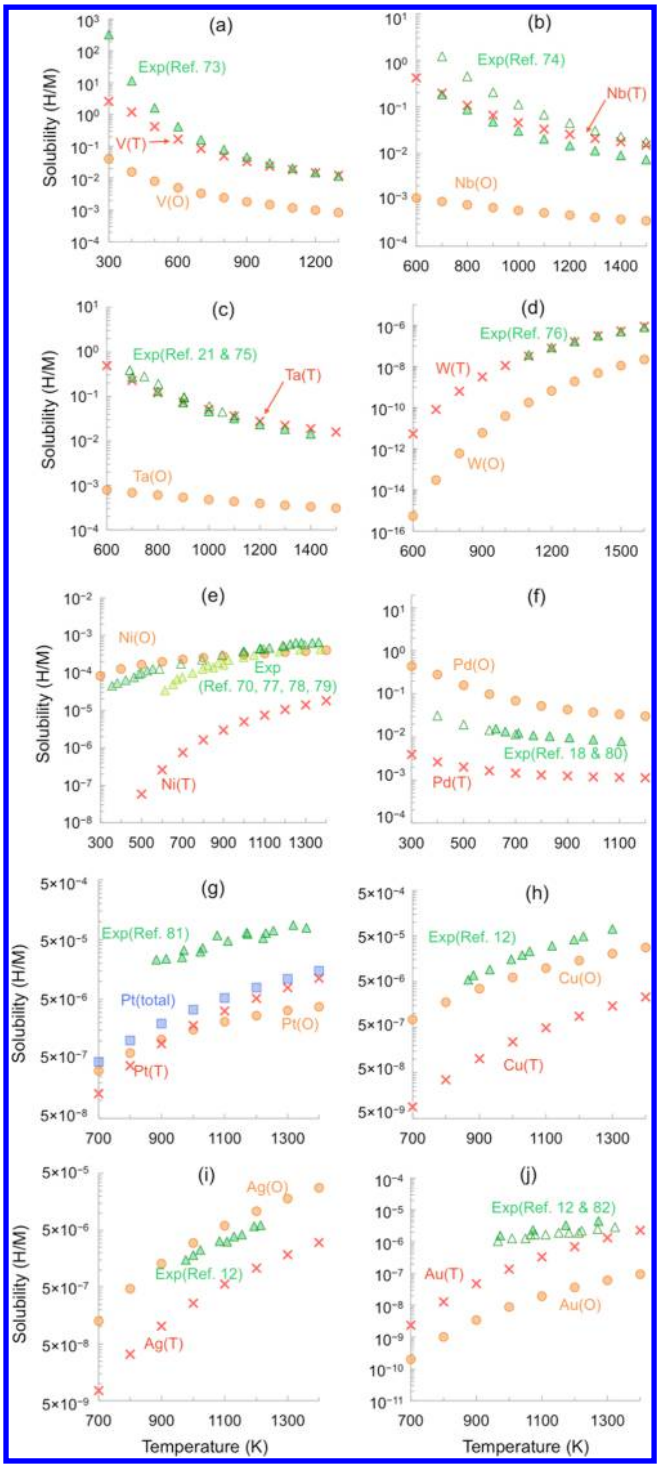

Figure 2. Hydrogen solubility in metals as a function of temperature predicted by first-principles calculations combined with thermodynamic equilibrium: (a) V, (b) Nb, (c) Ta, (d) W, (e) Ni, (f) Pd, (g) Pt, (h) Cu, (i) Ag, and (j) Au. Labels are color-coded following the associated plots.

with the O-site binding is in close proximity to that with the T-site binding, the sum of those solubilities is presented for comparison (Figure 2(g)). In Au, the T-site binding is stronger and is shown to dominate the solubility (Figure 2(h)).

The plots of the hydrogen solubility in the T-site of the BCC metals (V, Nb, Ta, and W) match the corresponding experimental results[21,73−76] very closely within a factor of 2. The predictions become much more accurate at higher temperatures (>1000 K), where the dilute solution assumption is more likely to be fulfilled (Figures 2(a), (b), (c), and (d)). Among the FCC metals, the experimental data on the hydrogen solubility in Ni,[70,77−79] Cu,[12] and Ag[12] match the solubilities predicted for the O-site binding within a factor of 3 (Figures 2(e), (h), and (i)). Larger deviations from experiments were observed in the cases of Pd,[18,80] Pt,[81] and Au[12,82] (Figures 2(f), (g), and (j)), which will be further discussed at the end of this section and in the following section.

Despite the difference in how well the DFT-predicted solubilities match with experimental data, some general trends can be observed. The Group 5 metals investigated exhibit very high solubilities compared to the other metals. On the other hand, Pd shows moderate solubility, and the late transition metals have very low solubilities, all of which agree well with the general trends in the experimental literature. Another feature in the solubility plots of Figure 2 is the trend with respect to temperature. Hydrogen solubilities in V, Nb, Ta, and Pd decrease with increasing temperature, whereas those in W, Ni, Pt, Cu, Ag, and Au increase with increasing temperature. These opposite trends may in part be correlated to the sign of the binding energy predicted (ZPE-corrected binding energy in Table 2) since the binding energy is equivalent to the enthalpy of dissolution (or absorption). A negative binding energy corresponds to exothermic dissolution, while a positive binding energy corresponds to endothermic dissolution. Strictly speaking, the solubility trend with temperature does not exactly correspond to the sign of the binding energy since the solubility is a function not only of binding energy but also of vibrational frequency. The mismatch between the sign of the binding energy and exothermicity may occur particularly when the absolute magnitude of the binding energy is substantially small (<ca. 0.05 eV/H). For instance, solubility predictions for the O-site of Nb and Ta present an exothermic trend even though the binding energies are slightly positive.

The poor predictability in the case of Pd has also been observed in Matsumoto et al., where the deviations were attributed to the hydrogen−hydrogen interactions within the high-concentration regime. On the other hand, the deviations in this study may be due to the errors associated with our vibrational frequency calculation. The vibrational frequency of a hydrogen atom in the O-site of bulk Pd measured by inelastic neutron scattering is 532 ± 32 cm^{-1},[83] deviating from our prediction by approximately 220 cm^{-1}, translating to an error of 42%. The errors may be partially attributed to the anharmonicity of the interstitial hydrogen potential in Pd.[84,85] In addition, tens of cm^{-1} are the typical error when vibrational frequencies are calculated by the finite displacement method using DFT.[71] At low vibrational frequencies as in this example, the relative error in vibrational frequency becomes high and generates a large error in the solubility predictions, as discussed in Section 3.1. Figure 3 shows a corrected prediction of the hydrogen solubility in Pd by applying the experimentally known vibrational frequency. The frequency correction lowered the solubility curve, resulting in a drastically improved match with the experimental solubility values. A deviation appearing at the low temperature range implies that the dilute solution assumption is violated as the hydrogen solubility increases, and the interaction between absorbed hydrogen atoms becomes non-negligible. The interaction may be repulsive, thereby constraining further hydrogen absorption as previously reported in the literature for highly concentrated systems.[25,86]

DOI: 10.1021/acs.jpcc.5b05469
J. Phys. Chem. C 2015, 119, 19642−19653

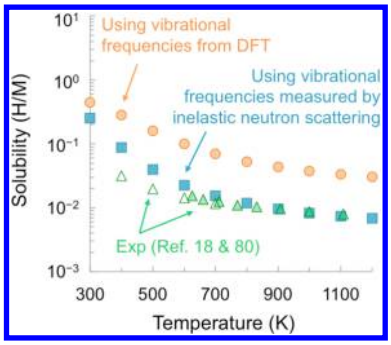

Figure 3. Hydrogen solubility in Pd corrected by applying experimental vibrational frequencies.

3.5. Interstitial Hydrogen in Pt and Au and Corrected Solubility. The deviated solubility prediction in Pt and Au shown in Figures 2(g) and (j) may also be attributed to the inaccuracies in vibrational frequency predictions. To the authors' knowledge, experimentally determined vibrational frequencies or evidence of the site preference of interstitial hydrogen in Pt or Au has not been reported in the literature. Several theoretical studies based on first-principles calculations have shown that the T-site is preferred in Au for hydrogen binding,[38,39,87] whereas other experimental studies presumed O-site binding for Pt and Au.[12,69,81] Some studies have reported that the hydrogen trapping in metal vacancy defects is favored over interstitial binding for Au and Pt.[88]

While we concluded a T-site preference of hydrogen binding in Pt and Au based on the binding energy and vibrational frequency calculations, there is a degree of uncertainty involved in this conclusion due to the interstitial size argument. In order to validate this unusual site preference in Pt and Au compared to other FCC metals, we attempted several investigations to enhance the accuracy of our force calculations, which is directly related to the normal-mode frequencies we would obtain.

First, we allowed the vibrations of the bulk metal atoms to be coupled with hydrogen vibrations during the frequency calculations and confirmed that the imaginary frequencies of the hydrogen vibrations changed by a small amount, i.e., 0.56% and 0.04% for Pt and Au, respectively. The calculated frequencies are given in Table 3.

Second, we adjusted the size of finite displacement from 0.015 to 0.007 Å and further to 0.001 Å during the vibrational frequency calculations to avoid the case in which a large displacement may place the hydrogen far beyond the energy minimum. However, imaginary frequencies were still obtained, as shown in Table 3. With a displacement size of 0.007 Å, the imaginary frequencies varied by −1.0 and −0.4% for Pt and Au, respectively, for the case of a displacement of 0.015 Å. With a displacement size of 0.001 Å, the three frequencies in each metal are not identical, in contrast to the cases of the two larger displacement sizes. This discrepancy may be due to the errors caused by numerical approximations associated with too small of a displacement size, which renders the corresponding energy difference to be too small for an accurate evaluation. Nevertheless, the changes in the imaginary frequencies compared to those with a displacement size of 0.015 Å are only −2.3 and −1.2% for Pt and Au, respectively.

Third, we applied a different method to the force calculation, i.e., density functional perturbation theory (DFPT),[89−91] in which normal-mode vibrational frequencies were calculated via a linear response method. We still observed imaginary

Table 3. Vibrational Frequencies of Hydrogen in the O-Site of Pt and Au, Calculated with Varying Parameters[a]

calculation condition	imaginary vibrational frequency/ i (cm^{-1})		
Pt			
all relaxed, d = 0.015 Å	399.5	399.5	399.6
only H relaxed, d = 0.015 Å	397.3	397.3	397.3
only H relaxed, d = 0.007 Å	393.1	393.2	393.7
only H relaxed, d = 0.001 Å	381.2	387.7	395.5
all relaxed, DFPT	396.9	396.9	396.9
only H relaxed, DFPT	392.8	392.8	392.8
Au			
all relaxed, d = 0.015 Å	449.1	450.0	449.9
only H relaxed, d = 0.015 Å	448.9	449.8	449.7
only H relaxed, d = 0.007 Å	447.2	447.3	447.9
only H relaxed, d = 0.001 Å	436.4	447.6	447.7
all relaxed, DFPT	448.6	448.6	448.6
only H relaxed, DFPT	447.4	447.4	447.4

[a]"d" denotes the size of the displacement in the vibrational frequency calculations using a finite displacement method.

frequencies for the hydrogen vibration in Pt of 392.8i and 396.9i cm^{-1} for hydrogen-only and all-atom relaxation cases, respectively. Similarly in Au, the two imaginary frequencies of 447.4i and 448.6i cm^{-1} were obtained for hydrogen-only and all-atom relaxation cases, respectively (Table 3). The values obtained by DFPT differ only by −1.1% and −0.5% from those calculated by the finite displacement method for Pt and Au, respectively.

In the fourth approach, we reoptimized the geometry of Pt and Au with a hydrogen atom occupying the O-site by imposing full lattice relaxation, and the results are shown in Table 4. We found that the lattice constants of Pt and Au

Table 4. Hydrogen Binding Energy and Vibrational Frequencies in the O-Site of Au and Pt Associated with Geometry Optimization and Supercell Extension[a]

supercell	lattice const. (Å)	BE (eV/H)	vibrational frequencies/i (cm^{-1})		
Pt					
2 × 2 × 2 (32 atoms), fixed lattice	3.98	0.58	397.3	397.3	397.3
2 × 2 × 2 (32 atoms), fully relaxed	3.99	0.57	410.7	410.6	410.7
3 × 3 × 3 (108 atoms), fully relaxed	3.98	0.56	406.1	407.7	407.8
Au					
2 × 2 × 2 (32 atoms), fixed lattice	4.17	1.03	448.9	449.8	449.7
2 × 2 × 2 (32 atoms), fully relaxed	4.18	1.02	456.8	457.7	457.6
3 × 3 × 3 (108 atoms), fully relaxed	4.18	1.00	432.9	434.1	434.1

[a]Only the H atom was displaced in the vibrational frequency calculations.

became 0.2% larger than those obtained from the fixed-lattice calculations. The normal-mode vibrational frequencies with this new geometry are still imaginary and are 3.4% and 1.8% higher for Pt and Au, respectively, than those calculated from a fixed geometry. The binding energies changed by only 0.01 eV.

The fifth approach was to increase the supercell size of Pt and Au from a 2 × 2 × 2 (32 atoms) to a 3 × 3 × 3 (108

DOI: 10.1021/acs.jpcc.5b05469
J. Phys. Chem. C 2015, 119, 19642−19653

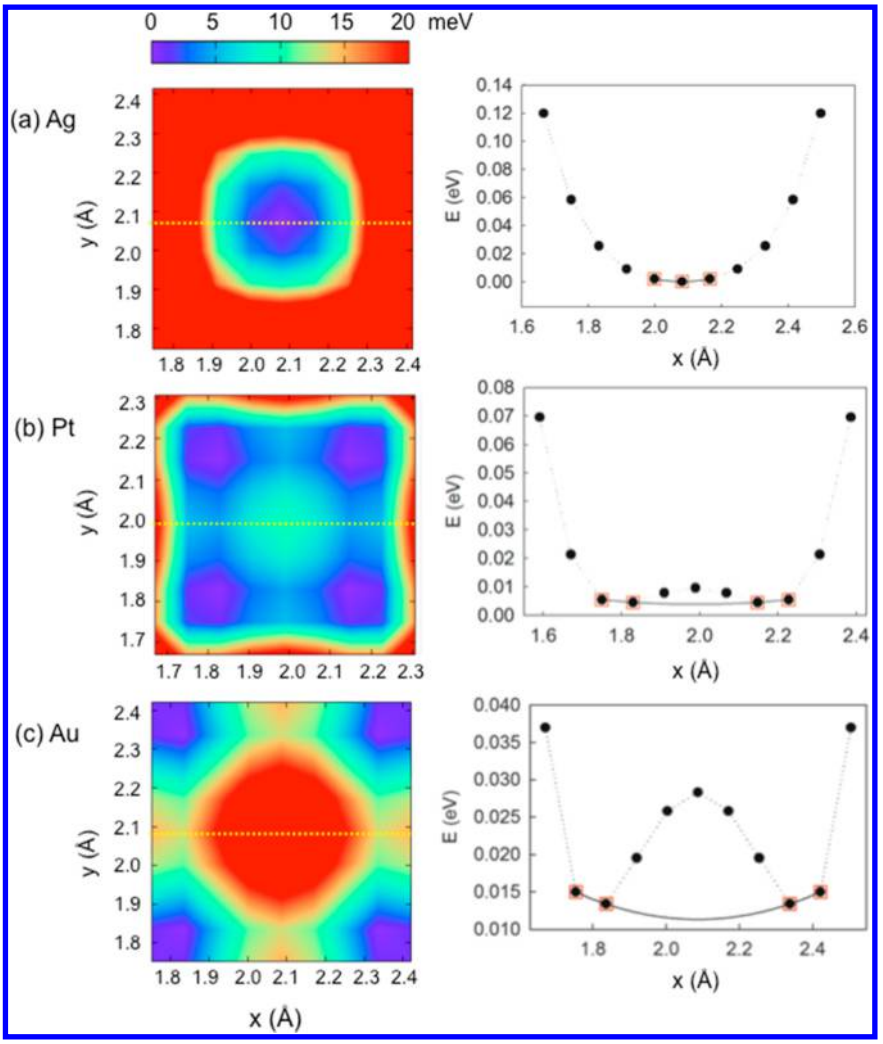

Figure 4. Potential energy surface projected onto the (002) surface of metals with the O-site at the center (left) and potential energy plotted along the dotted line on the potential energy surface (right): (a) Ag, (b) Pt, and (c) Au.

atoms) conventional unit cell. The rationale was that this may allow for the elimination of fictitious interactions between hydrogen atoms through periodic images. Nevertheless, the binding energies and vibrational frequencies hardly changed, as shown in Table 4.

As a final approach to understand the origin of the imaginary frequencies, we constructed a PES based on fixed-geometry calculations. In other words, for each data point on the PES, the total energy was calculated with a fixed geometry, where the metal atoms were fixed and only the hydrogen atom was displaced from the optimized geometry. After the calculation of each data point, the hydrogen atom was displaced from its previous position on the plane of a normal-mode vibration by 2% of the lattice constant of the corresponding metal. Since the metal atom positions would merely change with such a small displacement of hydrogen in reality, the PES we generated would describe the energy landscape near the hydrogen binding site. We chose Ag as a reference case to be compared with for several reasons: no imaginary frequencies were observed in Ag, the DFT-predicted solubility matches well with the experimental values, and the lattice constant of Ag is close to that of Au. Shown in Figure 4 are the PESs that are projected onto the (002) surface, on which the O-site is located at the center with a normal-mode vibration indicated by a dotted line.

The x- and y-coordinates of the plots range within ±10% of each metal's lattice constant, and the energy level is color-coded within a range of 0−20 meV. We also present a plot associated with each PES, showing the energy values along the yellow dotted line drawn on the PES. We assumed that one of the normal modes of vibration would exist along this dotted line since this is the case in all the other FCC metals investigated.

While the PES of Ag−H appears as a smooth basin (Figure 4(a)), Pt−H (Figure 4(b)) and Au−H (Figure 4(c)) possess much shallower PESs that are kinked across the O-site. The centers of the O-sites in Pt and Au are shown to be at higher energies than the minima on the (002) plane by 5 and 15 meV, respectively. Those fluctuations on the shallow basins, particularly the local maximum on the center of the PES, explain why imaginary frequencies have occurred in the previous calculations presented in Section 3.3. To find the true minima, a hydrogen atom was placed near the minima in Pt and Au on the PESs (the purple color region in the PESs), and geometry optimization was performed. Binding energies of hydrogen in the new sites in Pt and Au were reduced by 0.02 and 0.04 eV, respectively. Vibrational frequencies of hydrogen in Pt (687.9, 626.2, and 365.3i cm^{-1}) and Au (802.5, 620.3, and 404.3i cm^{-1}) calculated by the finite displacement method with a displacement size of 0.015 Å then showed only one imaginary

DOI: 10.1021/acs.jpcc.5b05469
J. Phys. Chem. C 2015, 119, 19642−19653

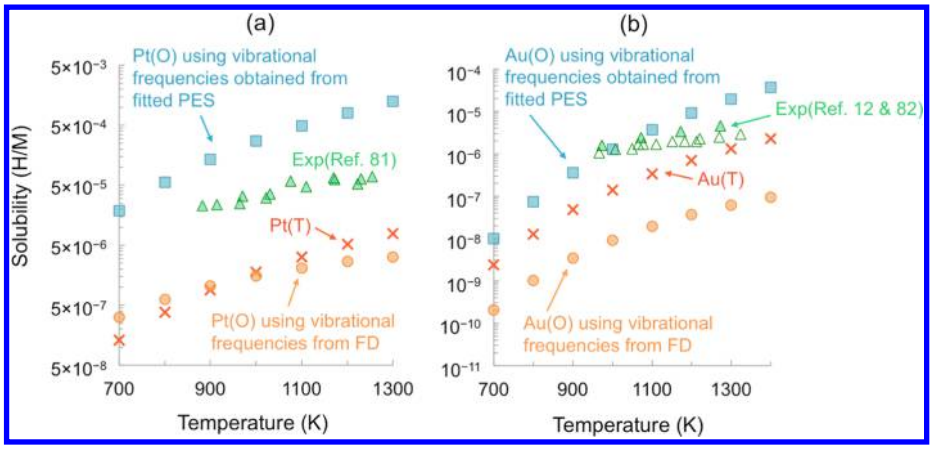

Figure 5. Modified hydrogen solubility in (a) Pt and (b) Au. The vibrational frequencies obtained from the finite displacement (FD) method and those obtained from the PES analysis were applied to calculate hydrogen solubility.

frequency instead of three. Therefore, these off-center O-sites are not the energy minima but first-order saddle points, which may be transition states along the paths of hydrogen diffusion in Pt and Au. Nazarov et al.[39] have also reported similar potential energy curves at the O-sites of Pt and Au, but they concluded that hydrogen in the Pt O-site is stable due to the ZPE contribution. Our vibrational frequency analysis indicates that the hydrogen at the Pt O-site is at a saddle point rather than a ground state.

While the magnitude of the fluctuations borders on the total energy convergence criteria specified in our DFT calculations (1 meV/atom), the vibrational frequency calculations have identified the correct PES features (first- versus third-order saddle point), implying that the calculation results are reasonably reliable. On the basis of all the tests attempted to improve the force calculations for hydrogen in the O-site of Pt and Au, it is strongly believed that the O-site would not be the stable binding sites for hydrogen in these two metals. The shallow basins featured on the PESs of Au and Pt (Figures 4(b) and (c)) mean that a very tight force convergence would be required to guarantee the accuracy of vibrational frequency calculations across the basin. We believe that the accuracy of our energy calculations is nearly at the limit of the PAW approximation. An all-electron method may improve the accuracy of force calculations, but the computations would be extremely demanding and impractical.

If we are to be more conservative and deduce that the fluctuations near the O-sites in Pt and Au are fictitious due to the intrinsic limit of DFT calculations, it would be rational to ignore the fluctuations. To justify the case, we calculated the hydrogen vibrational frequency by fitting only 3−4 legitimate PES data points (indicated by red squares on the plots in Figure 4) to satisfy the small displacement condition, assuming that a harmonic vibration would reasonably describe the hydrogen vibrations in the O-site. We assumed that the normal-mode vibrational frequencies along the other two directions would be identical to the frequency we calculated from the fitting due to the site symmetry in the FCC metals. The PES of Ag−H fits the harmonic vibration assumption reasonably well (Figure 4(a)), and the vibrational frequency of hydrogen in Ag was estimated to be 389.5 cm^{-1}, remarkably close to the result obtained by the finite displacement method (380.3 cm^{-1}). The estimated hydrogen vibrational frequencies in Pt and Au are 123.8 and 133.0 cm^{-1}, respectively.

We applied these frequency values in the hydrogen solubility calculations and plotted the updated solubilities as shown in Figure 5. Compared to the solubilities predicted from the vibrational frequencies calculated by the finite displacement method, the O-site solubility increased by 2−3 orders of magnitude in both Pt and Au. In Pt (Figure 5(a)), the updated O-site solubilities exceed the experimentally known solubilities but have become slightly closer to the experimental values than before the vibrational frequency correction. Nevertheless, the deviations are greater than an order of magnitude. In Au (Figure 5(b)), the O-site solubility became closer to the experimentally known solubility after the frequency correction, but the difference between the O- and T-site solubility estimates is within an order of magnitude, leaving the site preference undetermined.

Both the Pt and Au cases demonstrate that relatively low vibrational frequencies of hydrogen (approximately 250−750 cm^{-1} lower than that in the other FCC metals) lead to a higher solubility in the O-site compared to the T-site, despite the unfavorable binding energy in the O-site. These are clear examples that the solubility depends not only on the binding energy but also on the vibrational frequency. If the vibrational frequency of hydrogen in Pt and Au could be measured experimentally in future work, it will become possible to validate theoretical predictions of the solubility as well as the site preference.

In future studies, an improvement could be to include vacancy defects for establishing the equilibrium of hydrogen solid solution, particularly for late transition metals including Au and Pt. Vacancy formation energy in those metals is significantly lower than in early and midtransition metals,[92] allowing for higher concentration of vacancies to be available for stronger hydrogen binding[39] and thereby dominating the total hydrogen solubility.

CONCLUSIONS

The hydrogen solubility in 10 transition metals (V, Nb, Ta, W, Ni, Pd, Pt, Cu, Ag, and Au) was predicted by first-principles-based calculations combined with the thermodynamic equilibrium assumption. We calculated the binding energy and vibrational frequencies of a hydrogen atom in metal interstitial sites by first-principles calculations based on DFT and applied those results to a solubility equation derived based on the chemical potential equilibrium between hydrogen in the gas

DOI: 10.1021/acs.jpcc.5b05469
J. Phys. Chem. C 2015, 119, 19642−19653

and solid-solution phases. In general, the solubility increases with increasing binding strength and decreasing vibrational frequencies of hydrogen. Stronger binding leads to a higher solubility, as more hydrogen will be absorbed in the metal due to the strong affinity. Smaller vibrational frequencies result in a larger vibrational partition function, leading to a higher solubility.

The accuracy of solubility is critically dependent on the calculated binding energy and vibrational frequency. We present the results of a sensitivity analysis quantitatively illustrating the impact of errors in binding energy and vibrational frequency calculations on the predicted solubility. For instance, in FCC metals, an error of 0.11 eV in the binding energy or 300−400 cm^{-1} in the vibrational frequency induces errors in the solubility by an order of magnitude.

Our binding energy results indicate the favorable hydrogen occupancy to be in the T-site of the BCC metals and in the O-site of the FCC metals with the exception of Pt and Au, which prefer binding in the T-site. All the binding site preference agrees well with previous experimental and theoretical studies. While vibrational frequency calculations have revealed three real vibrational frequencies in most of the interstitial binding sites, the O-site of the BCC metals appears to be a second-order saddle point due to the high-energy configuration in the tight O-site geometry. Across the center of the O-site in Pt and Au, the PESs have revealed a very shallow energy difference and particularly have shown a slightly downward concavity at the center, causing only imaginary vibrational frequencies to occur. At the local energy minima near those O-sites, first-order saddle points were identified by the presence of one imaginary vibrational frequency. Harmonic vibrational frequencies obtained from fitting the PESs appeared to be very low both for Pt and Au (120−130 cm^{-1}), as expected from the shallow feature of the PES.

Our hydrogen solubility predictions matched experimentally known solubility data from the literature within a factor of 2 in the cases of V, Nb, Ta, and W and within a factor of 3 in the cases of Ni, Cu, and Ag. Larger deviations from experimental data were found in Pd, mainly due to the errors associated with vibrational frequency calculations. By applying the experimental vibrational frequency of hydrogen to the solubility calculation, the predicted solubility in Pd was significantly improved and matched the experimental solubility. The reasons for the deviations in the hydrogen solubility predictions for Pt and Au remain uncertain, since no experimental evidence of the vibrational frequencies or site preference is available. Applying the harmonic vibrational frequencies of hydrogen estimated from the smoothened PESs to Pt and Au merely improved the solubility predictions. Future studies that measure the hydrogen vibration in the interstitial sites of Pt and Au may provide a good reference to this study, thereby improving the solubility predictions. The methodology to predict hydrogen solubility in this study may be applied to more complicated systems such as alloys or used to estimate the solubilities of other solutes or impurities in metallic systems.

■ ASSOCIATED CONTENT

Supporting Information

The Supporting Information is available free of charge on the ACS Publications website at DOI: 10.1021/acs.jpcc.5b05469.

Details of solubility calculations and derivations (PDF)

■ AUTHOR INFORMATION

Corresponding Author

*Tel.: (650)724-9449. Fax: (650)725-2099. E-mail: jen.wilcox@stanford.edu.

Notes

The authors declare no competing financial interest.

■ ACKNOWLEDGMENTS

We would like to thank Dr. Dawn Geatches and Dr. Chun-Yaung Lu for their thorough review of the manuscript and helpful discussion. We acknowledge the high performance computing (HPC) facilities in the Center for Computational Earth and Environmental Science (CEES) at Stanford University. This work has received financial support from NSF Grant 1263991.

■ REFERENCES

(1) Basile, A.; Gallucci, F.; Tosti, S. Synthesis, Characterization, and Applications of Palladium Membranes. In *Fundamentals of Inorganic Membrane Science and Technology*; Reyes, M., Miguel, M., Eds.; Elsevier: New York, 2008; Vol. *13*, pp 255−323.

(2) Dolan, M. D. Non-Pd Bcc Alloy Membranes for Industrial Hydrogen Separation. *J. Membr. Sci.* **2010**, *362*, 12−28.

(3) Dolan, M. D.; Dave, N. C.; Ilyushechkin, A. Y.; Morpeth, L. D.; McLennan, K. G. Composition and Operation of Hydrogen-Selective Amorphous Alloy Membranes. *J. Membr. Sci.* **2006**, *285*, 30−55.

(4) Hatlevik, Ø.; Gade, S. K.; Keeling, M. K.; Thoen, P. M.; Davidson, A. P.; Way, J. D. Palladium and Palladium Alloy Membranes for Hydrogen Separation and Production: History, Fabrication Strategies and Current Performance. *Sep. Purif. Technol.* **2010**, *73*, 59−64.

(5) Paglieri, S. N.; Way, J. D. Innovations in Palladium Membrane Research. *Sep. Purif. Rev.* **2002**, *31*, 1−171.

(6) Wipf, H. Solubility and Diffusion of H in Pure Metals and Alloys. *Phys. Scr.* **2001**, *T94*, 43−51.

(7) Bernstein, I. M. The Role of Hydrogen: Is the Story Any Clearer? In *Hydrogen Effects in Materials*; Thompson, A. W., Moody, N. R., Eds.; The Minerals, Metals, & Materials Society: Warrendale, PA, 1996; pp 3−11.

(8) Wang, J. S. Hydrogen Induced Embrittlement and the Effect of the Mobility of Hydrogen Atoms. In *Hydrogen Effects in Materials*; Thompson, A. W., Moody, N. R., Eds.; The Minerals, Metals, & Materials Society: Warrendale, PA, 1996; pp 61−75.

(9) Oates, W. A.; McLellan, R. B. The Solubility of H in Mo. *Scr. Metall.* **1972**, *6*, 349−352.

(10) Holleck, G. L. Diffusion and Solubility of Hydrogen in Palladium and Palladium-Silver Alloys. *J. Phys. Chem.* **1970**, *74*, 503−511.

(11) Chang, H. Y.; Wert, C. A. The Solubility and Trapping of Hydrogen in Vanadium. *Acta Metall.* **1973**, *21*, 1233−1242.

(12) McLellan, R. B. Solid Solutions of Hydrogen in Gold, Silver and Copper. *J. Phys. Chem. Solids* **1973**, *34*, 1137−1141.

(13) Perkins, W. G. Permeation and Outgassing of Vacuum Materials. *J. Vac. Sci. Technol.* **1973**, *10*, 543−556.

(14) Westlake, D. G.; Miller, J. F. Terminal Solubility of Hydrogen in Nb-Ta Alloys and Characterization of the Solid Solutions. *J. Less-Common Met.* **1979**, *65*, 139−154.

(15) Katsuta, H.; McLellan, R. B. Diffusivity Permeability and Solubility of Hydrogen in Platinum. *J. Phys. Chem. Solids* **1979**, *40*, 697−699.

(16) Flanagan, T. B.; Lynch, J. F.; Clewley, J. D.; Von Turkovich, B. The Effect of Lattice Defects on Hydrogen Solubility in Palladium: I. Experimentally Observed Solubility Enhancements and Thermodynamics of Absorption. *J. Less-Common Met.* **1976**, *49*, 13−24.

(17) Langeberg, J. C.; McLellan, R. B. Thermodynamics of Bcc Solid Solutions of Hydrogen in Niobium, Vanadium and Tantalum. *Acta Metall.* **1973**, *21*, 897−902.

DOI: 10.1021/acs.jpcc.5b05469
J. Phys. Chem. C 2015, 119, 19642−19653

(18) Weiss, A.; Ramaprabhu, S.; Rajalakshmi, N. Hydrogen Solubility and Thermodynamics of Hydrogen Absorption in Palladium-Rich Binary $Pd_{1-x}Z_x$ and Ternary $Pd_{1-x-y}Z_xZ'_y$ Solid Solution Alloys. *Z. Phys. Chem.* **1997**, *199*, 165−212.
(19) Fukai, Y. *The Metal-Hydrogen System: Basic Bulk Properties*; Springer Science & Business Media: New York, 2006.
(20) McLellan, R. B.; Harkins, C. G. Hydrogen Interactions with Metals. *Mater. Sci. Eng.* **1975**, *18*, 5−35.
(21) Ebisuzaki, Y.; O'Keeffe, M. The Solubility of Hydrogen in Transition Metals and Alloys. *Prog. Solid State Chem.* **1967**, *4*, 187−211.
(22) Lee, H. M. The Solubility of Hydrogen in Transition Metals. *Metall. Trans. A* **1976**, *7*, 431−433.
(23) Oates, W. A.; Flanagan, T. B. The Solubility of Hydrogen in Transition Metals and Their Alloys. *Prog. Solid State Chem.* **1981**, *13*, 193−272.
(24) Nørskov, J. K.; Besenbacher, F. Theory of Hydrogen Interaction with Metals. *J. Less-Common Met.* **1987**, *130*, 475−490.
(25) Matsumoto, R.; Sera, M.; Miyazaki, N. Hydrogen Concentration Estimation in Metals at Finite Temperature Using First-Principles Calculations and Vibrational Analysis. *Comput. Mater. Sci.* **2014**, *91*, 211−222.
(26) Kamakoti, P.; Sholl, D. A Comparison of Hydrogen Diffusivities in Pd and CuPd Alloys Using Density Functional Theory. *J. Membr. Sci.* **2003**, *225*, 145−154.
(27) Kamakoti, P.; Morreale, B. D.; Ciocco, M. V.; Howard, B. H.; Killmeyer, R.; Cugini, A. V.; Sholl, D. S. Prediction of Hydrogen Flux through Sulfur-Tolerant Binary Alloy Membranes. *Science* **2005**, *307*, 569−573.
(28) Sonwane, C. G.; Wilcox, J.; Ma, Y. H. Solubility of Hydrogen in PdAg and PdAu Binary Alloys Using Density Functional Theory. *J. Phys. Chem. B* **2006**, *110*, 24549−24558.
(29) Semidey-Flecha, L.; Sholl, D. S. Combining Density Functional Theory and Cluster Expansion Methods to Predict H_2 Permeance through Pd-Based Binary Alloy Membranes. *J. Chem. Phys.* **2008**, *128*, 144701−144710.
(30) Qin, L.; Jiang, C. First-Principles Based Modeling of Hydrogen Permeation through Pd-Cu Alloys. *Int. J. Hydrogen Energy* **2012**, *37*, 12760−12764.
(31) Liu, Y.-L.; Zhou, H.-B.; Zhang, Y. Investigating Behaviors of H in a W Single Crystal by First-Principles: From Solubility to Interaction with Vacancy. *J. Alloys Compd.* **2011**, *509*, 8277−8282.
(32) Kong, X.-S.; Wang, S.; Wu, X.; You, Y.-W.; Liu, C. S.; Fang, Q. F.; Chen, J.-L.; Luo, G. N. First-Principles Calculations of Hydrogen Solution and Diffusion in Tungsten: Temperature and Defect-Trapping Effects. *Acta Mater.* **2015**, *84*, 426−435.
(33) Liu, Y.-L.; Jin, S.; Sun, L.; Duan, C. First-Principles Investigation on Diffusion and Permeation Behaviors of Hydrogen Isotopes in Molybdenum. *Comput. Mater. Sci.* **2012**, *54*, 32−36.
(34) Zhou, H.-B.; Zhang, Y.; Ou, X. Dissolution and Diffusion Behaviors of Hydrogen in Copper: A First-Principles Investigation. *Comput. Mater. Sci.* **2013**, *79*, 923−928.
(35) Zhou, H.-B.; Liu, Y.-L.; Jin, S.; Zhang, Y.; Luo, G. N.; Lu, G.-H. Investigating Behaviours of Hydrogen in a Tungsten Grain Boundary by First Principles: From Dissolution and Diffusion to a Trapping Mechanism. *Nucl. Fusion* **2010**, *50*, 025016.
(36) Ohsawa, K.; Eguchi, K.; Watanabe, H.; Yamaguchi, M.; Yagi, M. Configuration and Binding Energy of Multiple Hydrogen Atoms Trapped in Monovacancy in Bcc Transition Metals. *Phys. Rev. B: Condens. Matter Mater. Phys.* **2012**, *85*, 094102.
(37) Gui, L.-J.; Liu, Y.-L.; Wang, W.-T.; Jin, S.; Zhang, Y.; Lu, G.-H.; Yao, J.-E. First-Principles Investigation on Vacancy Trapping Behaviors of Hydrogen in Vanadium. *J. Nucl. Mater.* **2013**, *442*, S688−S693.
(38) You, Y.-W.; Kong, X.-S.; Wu, X.-B.; Xu, Y.-C.; Fang, Q. F.; Chen, J. L.; Luo, G.-N.; Liu, C. S.; Pan, B. C.; Wang, Z. Dissolving, Trapping and Detrapping Mechanismsof Hydrogen in Bcc and Fcc Transition Metals. *AIP Adv.* **2013**, *3*, 012118.
(39) Nazarov, R.; Hickel, T.; Neugebauer, J. Ab Initio Study of H-Vacancy Interactions in Fcc Metals: Implications for the Formation of Superabundant Vacancies. *Phys. Rev. B: Condens. Matter Mater. Phys.* **2014**, *89*, 144108.
(40) Fukai, Y.; Okuma, N. Formation of Superabundant Vacancies in Pd Hydride under High H2 Pressures. *Phys. Rev. Lett.* **1994**, *73*, 1640−1643.
(41) Fukai, Y. Formation of Superabundant Vacancies in M−H Alloys and Some of Its Consequences: A Review. *J. Alloys Compd.* **2003**, *365*−*357*, 263−269.
(42) Hohenberg, P.; Kohn, W. Inhomogeneous Electron Gas. *Phys. Rev.* **1964**, *136*, B864−B871.
(43) Kohn, W.; Sham, L. J. Self-Consistent Equations Including Exchange and Correlation Effects. *Phys. Rev.* **1965**, *140*, A1133−A1138.
(44) Kresse, G.; Furthmuller, J. Efficient Iterative Schemes for Ab Initio Total-Energy Calculations Using a Plane-Wave Basis Set. *Phys. Rev. B: Condens. Matter Mater. Phys.* **1996**, *54*, 11169.
(45) Kresse, G.; Furthmüller, J. Efficiency of Ab-Initio Total Energy Calculations for Metals and Semiconductors Using a Plane-Wave Basis Set. *Comput. Mater. Sci.* **1996**, *6*, 15−50.
(46) Kresse, G.; Hafner, J. Ab Initio Molecular Dynamics for Open-Shell Transition Metals. *Phys. Rev. B: Condens. Matter Mater. Phys.* **1993**, *48*, 13115.
(47) Kresse, G.; Hafner, J. Ab Initio Molecular-Dynamics Simulation of the Liquid-Metal-Amorphous-Semiconductor Transition in Germanium. *Phys. Rev. B: Condens. Matter Mater. Phys.* **1994**, *49*, 14251.
(48) Blöchl, P. E. Projector Augmented-Wave Method. *Phys. Rev. B: Condens. Matter Mater. Phys.* **1994**, *50*, 17953−17979.
(49) Kresse, G.; Joubert, D. From Ultrasoft Pseudopotentials to the Projector Augmented-Wave Method. *Phys. Rev. B: Condens. Matter Mater. Phys.* **1999**, *59*, 1758−1775.
(50) Perdew, J. P.; Burke, K.; Ernzerhof, M. Generalized Gradient Approximation Made Simple. *Phys. Rev. Lett.* **1996**, *77*, 3865−3868.
(51) Perdew, J. P.; Burke, K.; Ernzerhof, M. Erratum: Generalized Gradient Approximation Made Simple. *Phys. Rev. Lett.* **1997**, *78*, 1396.
(52) Monkhorst, H. J.; Pack, J. D. Special Points for Brillouin-Zone Integrations. *Phys. Rev. B* **1976**, *13*, 5188−5192.
(53) Methfessel, M.; Paxton, A. T. High-Precision Sampling for Brillouin-Zone Integration in Metals. *Phys. Rev. B: Condens. Matter Mater. Phys.* **1989**, *40*, 3616−3621.
(54) Haas, P.; Tran, F.; Blaha, P. Calculation of the Lattice Constant of Solids with Semilocal Functionals. *Phys. Rev. B: Condens. Matter Mater. Phys.* **2009**, *79*, 085104.
(55) Tran, F.; Laskowski, R.; Blaha, P.; Schwarz, K. Performance on Molecules, Surfaces, and Solids of the Wu-Cohen Gga Exchange-Correlation Energy Functional. *Phys. Rev. B: Condens. Matter Mater. Phys.* **2007**, *75*, 115131.
(56) Aboud, S.; Wilcox, J. A Density Functional Theory Study of the Charge State of Hydrogen in Metal Hydrides. *J. Phys. Chem. C* **2010**, *114*, 10978−10985.
(57) Ouyang, C.; Lee, Y.-S. Hydrogen-Induced Interactions in Vanadium from First-Principles Calculations. *Phys. Rev. B: Condens. Matter Mater. Phys.* **2011**, *83*, 045111.
(58) Sundell, P.; Wahnström, G. Self-Trapping and Diffusion of Hydrogen in Nb and Ta from First Principles. *Phys. Rev. B: Condens. Matter Mater. Phys.* **2004**, *70*, 224301.
(59) Liu, Y.-L.; Zhang, Y.; Zhou, H.-B.; Lu, G.-H.; Liu, F.; Luo, G. N. Vacancy Trapping Mechanism for Hydrogen Bubble Formation in Metal. *Phys. Rev. B: Condens. Matter Mater. Phys.* **2009**, *79*, 172103.
(60) Heinola, K.; Ahlgren, T. Diffusion of Hydrogen in Bcc Tungsten Studied with First Principle Calculations. *J. Appl. Phys.* **2010**, *107*, 113531.
(61) Jiang, B.; Wan, F. R.; Geng, W. T. Strong Hydrogen Trapping at Helium in Tungsten: Density Functional Theory Calculations. *Phys. Rev. B: Condens. Matter Mater. Phys.* **2010**, *81*, 134112.
(62) Johnson, D. F.; Carter, E. A. Hydrogen in Tungsten: Absorption, Diffusion, Vacancy Trapping, and Decohesion. *J. Mater. Res.* **2010**, *25*, 315−327.

DOI: 10.1021/acs.jpcc.5b05469
J. Phys. Chem. C 2015, 119, 19642−19653

(63) Grena, R.; Celino, M.; Pietro, T. DFT Study of Interstitial Hydrogen in Tantalum Lattice. *Int. J. Hydrogen Energy* **2011**, *36*, 13858−13865.
(64) Wimmer, E.; Wolf, W.; Sticht, J.; Saxe, P.; Geller, C.; Najafabadi, R.; Young, G. Temperature-Dependent Diffusion Coefficients from Ab Initio Computations: Hydrogen, Deuterium, and Tritium in Nickel. *Phys. Rev. B: Condens. Matter Mater. Phys.* **2008**, *77*, 134305.
(65) Ke, X.; Kramer, G. Absorption and Diffusion of Hydrogen in Palladium-Silver Alloys by Density Functional Theory. *Phys. Rev. B: Condens. Matter Mater. Phys.* **2002**, *66*, 184304.
(66) Yokoi, Y.; Seki, T.; Yasuda, I. A First-Principles Study of Hydrogen Dissolution in Various Metals and Palladium-Silver Alloys. In *Adv. Hydrogen Energy*; Padro, G. C. E., Ed.; Springer: New York, 2000; pp 111−119.
(67) *Crc Handbook of Chemistry and Physics*, 94th ed.; CRC Press: Boca Raton, FL, 2013.
(68) Slater, J. C. Atomic Radii in Crystals. *J. Chem. Phys.* **1964**, *41*, 3199−3204.
(69) Driessen, A.; Sänger, P.; Hemmes, H.; Griessen, R. Metal Hydride Formation at Pressures up to 1 Mbar. *J. Phys.: Condens. Matter* **1990**, *2*, 9797−9814.
(70) McLellan, R. B.; Oates, W. A. The Solubility of Hydrogen in Rhodium, Ruthenium, Iridium and Nickel. *Acta Metall.* **1973**, *21*, 181−185.
(71) Wong, M. W. Vibrational Frequency Prediction Using Density Functional Theory. *Chem. Phys. Lett.* **1996**, *256*, 391−399.
(72) Jiang, D.; Carter, E. Diffusion of Interstitial Hydrogen into and through Bcc Fe from First Principles. *Phys. Rev. B: Condens. Matter Mater. Phys.* **2004**, *70*, 064102.
(73) Peterson, D. T.; Nelson, S. O. Isopiestic Solubility of Hydrogen in Vanadium Alloys at Low Temperatures. *Metall. Trans. A* **1985**, *16*, 367−374.
(74) Steward, S. A. *Review of Hydrogen Isotope Permeability through Materials* **1983**, 1−28.
(75) Sieverts, A.; Bergner, E. Tantalum, Tungsten and Hydrogen. *Ber. Dtsch. Chem. Ges.* **1911**, *44*, 2394−2402.
(76) Frauenfelder, R. Solution and Diffusion of Hydrogen in Tungsten. *J. Vac. Sci. Technol.* **1969**, *6*, 388−397.
(77) Stafford, S. W.; McLellan, R. B. The Solubility of Hydrogen in Nickel and Cobalt. *Acta Metall.* **1974**, *22*, 1463−1468.
(78) McLellan, R. B.; Sutter, P. L. Thermodynamics of the Hydrogen-Nickel System. *Acta Metall.* **1984**, *32*, 2233−2239.
(79) Smittenberg, J. Absorption and Adsorption of Hydrogen by Nickel. *Recl. Trav. Chim. Pays-Bas* **1934**, *53*, 1065−1083.
(80) Yoshihara, M.; McLlellan, R. B. Thermodynamics of Pd-Cu-H Solid Solutions. *Acta Metall.* **1983**, *31*, 61−68.
(81) Yei, W. M.; McLellan, R. B. Thermodynamics of Dilute Platinum-Hydrogen Solid Solutions. *J. Less-Common Met.* **1979**, *64*, 11−16.
(82) Okamoto, H.; Massalski, T. B. The Au-H (Gold-Hydrogen) System. *Bull. Alloy Phase Diagrams* **1985**, *6*, 365.
(83) Mitchell, P. C. H.; Parker, S. F.; Ramirez-Cuesta, A. J.; Tomkinson, J. Surface Chemistry and Catalysis. *Vibrational Spectroscopy with Neutrons*; World Scientific: Singapore, 2005; pp 285−336
(84) Oates, W. A.; Flanagan, T. B. Isotope Effect for the Solution of Hydrogen in Metals: Application to Pd/H(D). *J. Chem. Soc., Faraday Trans. 1* **1977**, *73*, 407−415.
(85) Oppeneer, P. M.; Lodder, A.; Griessen, R. Vibrations of Hydrogen Isotopes in Pd and the Consequences of Anharmonicity. *J. Phys. F: Met. Phys.* **1988**, *18*, 1733−1742.
(86) Hao, S.; Widom, M.; Sholl, D. S. Probing Hydrogen Interactions with Amorphous Metals Using First-Principles Calculations. *J. Phys.: Condens. Matter* **2009**, *21*, 115402.
(87) Järvi, T. T.; van Duin, A. C. T.; Nordlund, K.; Goddard, I. W. A. Development of Interatomic ReaxFF Potentials for Au−S−C−H Systems. *J. Phys. Chem. A* **2011**, *115*, 10315−10322.
(88) Gaskey, J. G. R.; Derrick, R. G. Trapping of Deuterium During Permeation through Gold. *Scr. Metall.* **1976**, *10*, 377−380.
(89) Baroni, S.; de Gironcoli, S.; Dal Corso, A.; Giannozzi, P. Phonons and Related Crystal Properties from Density-Functional Perturbation Theory. *Rev. Mod. Phys.* **2001**, *73*, 515−562.
(90) Baroni, S.; Giannozzi, P.; Testa, A. Green's-Function Approach to Linear Response in Solids. *Phys. Rev. Lett.* **1987**, *58*, 1861−1864.
(91) Giannozzi, P.; de Gironcoli, S.; Pavone, P.; Baroni, S. Ab Initio Calculation of Phonon Dispersions in Semiconductors. *Phys. Rev. B: Condens. Matter Mater. Phys.* **1991**, *43*, 7231−7242.
(92) Korhonen, T.; Puska, M. J.; Nieminen, R. M. Vacancy-Formation Energies for FCC and BCC Transition Metals. *Phys. Rev. B: Condens. Matter Mater. Phys.* **1995**, *51*, 9526−9532.

DOI: 10.1021/acs.jpcc.5b05469
J. Phys. Chem. C 2015, 119, 19642−19653